Dissipative particle dynamics as a computational tool to detect the morphology-rheology interplay in Pluronic F68/water mixtures: A promising drug carrier

Journal of Colloid and Interface Science 700 (2025) 138525

Contents lists available at ScienceDirect

Journal of Colloid And Interface Science

journal homepage: www.elsevier.com/locate/jcis

Regular Article

Dissipative particle dynamics as a computational tool to detect the morphology-rheology interplay in Pluronic F68/water mixtures: A promising drug carrier

N. Lauriello [a,*], N.A. Di Spirito [b,c], Karel Šindelka [d], G. Boccardo [a], R. Pasquino [b], N. Grizzuti [b], D. Marchisio [a]

[a] DISAT – Institute of Chemical Engineering, Politecnico di Torino, C.so Duca degli Abruzzi 24, Torino, 10129, Italy
[b] DICMaPI – Università degli Studi di Napoli Federico II, P.le Tecchio 80, Napoli, 80125, Italy
[c] Department of Engineering – Università degli Studi del Sannio, Corso Garibaldi 107, Benevento, 82100, Italy
[d] Department of Molecular and Mesoscopic Modelling – The Czech Academy of Sciences, Institute of Chemical Process Fundamentals, Rozvojová, Prague, 135/1, Czech Republic

GRAPHICAL ABSTRACT

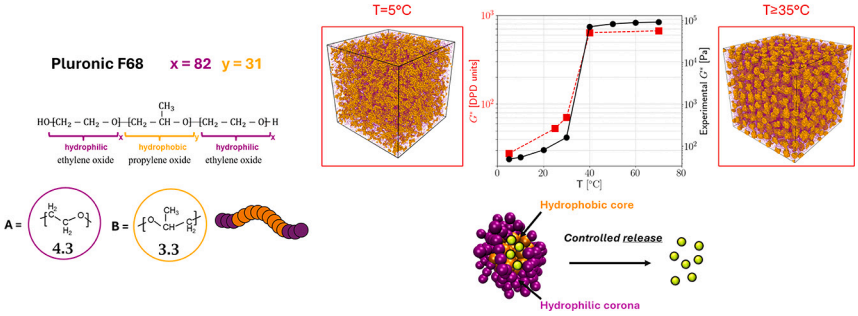

ARTICLE INFO

Keywords:
Dissipative particle dynamics
Rheology
Pluronics
Self-assembly
Drug delivery systems

ABSTRACT

Pluronics, also known as poloxamers, are amphiphilic triblock copolymers widely employed in drug delivery systems due to their tunable self-assembly and biocompatibility. Among them, Pluronic F68 (Poloxamer 188) exhibits thermoresponsive behavior in aqueous solution, forming ordered supramolecular structures at high concentrations and temperatures. In this work, we investigate the morphological and rheological properties of a 45 wt% Pluronic F68 aqueous system at different temperatures through a combination of experimental and computational approaches. Rheological measurements and Small-Angle X-ray Scattering (SAXS) confirm the formation of a body-centered cubic (BCC) structure at higher temperatures and highlight the emergence of viscoelastic solid-like behavior. To support and extend these findings, Dissipative Particle Dynamics (DPD) simulations are employed to model the nanostructure evolution and the impact of temperature on self-assembly and material properties. This integrated approach provides a consistent framework to characterize the temperature-induced transition from fluid-like to solid-like states and sets the groundwork for future simulation studies incorporating drug cargo. The results offer valuable insights into the design of thermoresponsive drug

* Corresponding author.
E-mail address: nunzia.lauriello@polito.it (N. Lauriello).

https://doi.org/10.1016/j.jcis.2025.138525
Received 19 May 2025; Received in revised form 8 July 2025; Accepted 22 July 2025

Available online 30 July 2025

delivery systems and demonstrate the potential of DPD in capturing complex structure–property relationships in amphiphilic polymer systems.

1. Introduction

Structured fluids are very common in food, personal-care and pharmaceutical industries and include polymeric solutions and melts, suspensions of colloidal particles, micellar solutions, and liquid foams. Among them, a peculiar class of amphiphilic materials, commercially known as Pluronics, has received increased attention over the last few years, since it offers a pool of more than fifty polymer-based polymorphic materials [1]. Pluronics, alias poloxamers, are triblock copolymers, composed of two lateral hydrophilic chains of polyethylene oxide (PEO) and a central hydrophobic chain of polypropylene oxide (PPO) [2]. The ability to precisely control the molecular characteristics of Pluronics, such as the PPO/PEO composition ratio, block lengths, and molecular weight, offers a high degree of tunability, allowing for the creation of macromolecules with tailored properties to meet specific application requirements. They are commonly referred to with an alphanumeric name consisting of a letter indicating the physical status and two digits indicating the molecular mass and composition. Such systems are widely used in industrial applications, as well as in more specialized uses in pharmaceutics and bioprocessing. Due to their biocompatibility, they are prominently featured in the development of nanocarriers for drug delivery [3].

Among these, Pluronic F68, also known as Poloxamer 188, has emerged as a promising drug carrier system, as demonstrated by previous experimental studies [4,3], due to its intriguing behavior at a concentration of 45% by weight (wt) at various temperatures. In fact, rheological measurements confirm that Pluronic F68 in water at high temperature takes the appearance of a soft solid, behaving as a non-Newtonian fluid with peculiar viscoelasticity. Notably, at elevated temperatures, the system exhibits a distinctive characteristic: it assembles into an ordered supramolecular structure known as the body-centered cubic (BCC) phase, resembling a solid-like structure. This observation has significant implications, especially in the realm of drug delivery systems. In fact, this system has been experimentally investigated [5,6], and the present modeling work lay the foundation for simulations that incorporate drug cargo. Although DPD has been applied in similar studies, the effects of temperature are often overlooked and neglected. On the contrary, in this system, temperature plays a crucial role.

The rheological, morphological, and structural properties of Pluronic F68 in water are investigated here to detect the influence of temperature on its linear viscoelastic behavior and supply knowledge on the nature and characteristic dimensions of the nanoassemblies.

The ability to adjust and control the morphology and rheological properties of drug delivery systems in which a pharmaceutical molecule is loaded is a hot topic in therapeutic applications where the release of a drug cargo in the human body needs to be controlled. The use of computational tools such as DPD, in conjunction with real experiments, allows to explore a wide range of scenarios, accelerating the design process. The properties of these materials, including the Critical Micellar Concentration (CMC) and the rheological behavior, need to be controlled and optimized for such applications. The CMC represents the concentration threshold at which self-assembly in micelles occurs, which impacts various functionalities, such as drug delivery. The rheological properties also play a crucial role in this application. Thus, predicting and controlling these properties is essential for optimizing their performance. However, this task is hindered by the time-consuming and costly experimental campaigns necessary to estimate the properties of the material, which are influenced by numerous variables such as composition, concentration, and temperature. In addition, capturing the interplay between morphology and material properties poses a significant challenge by relying only on theory and experiments. In this context, computational tools offer an intriguing alternative: they facilitate the mimicking of various scenarios rapidly and cost-effectively, providing a faster understanding on the effects of structural changes on final rheological properties.

Several computational models have been developed to describe the behavior of these fluids at different levels of representation. Among them, Dissipative Particle Dynamics (DPD) is one of the most widely utilized methods for investigating the behavior of these materials and predicting their properties. It is a mesoscopic technique that operates at time and length scales which would be inaccessible by using molecular-level methods and are relevant to capture the evolution of the morphologies that dictate the final materials properties. One of the reasons for this is that DPD is a coarse-grained (CG) model, where groups of atoms and molecules are treated as single entities called *beads*, interacting via a mesoscopic force field, made of conservative soft-repulsive and non-conservative interactions. The internal degrees-of-freedom of the molecules that a *bead* is intended to represent are included in an averaged way or effectively ignored. The computational advantages offered by DPD make it particularly appealing for simulating systems containing polymer chains, such as Pluronics in water.

This study conducts DPD simulations of systems composed by 45 wt% of Pluronic F68 and water. To ensure the reliability and validity of the simulation results, they are compared and validated against experimental data obtained from scattering techniques and rheological measurements, used to characterize the nanostructure and rheological properties of the system under similar conditions.

The combined experimental–computational framework clarifies the microstructural mechanisms underlying elasticity and, more broadly, the rheological behavior. In fact, the origin of elasticity in these compact micellar structures formed by poloxamers remains poorly understood and has been previously discussed in the literature [7,8]. The three-dimensional order of the BCC domain plays a crucial role, as mechanical deformation causes spherical micelles to shift from their equilibrium lattice positions, similar to those of simple three-dimensional crystalline solids, while thermodynamic forces restore them, preserving macrocrystalline order under static conditions. Hvidt et al. [9] proposed that the shear modulus is proportional to the interfacial tension between PPO and water, the micelle concentration and the square of the micelle radius. Alternatively, Lau et al. [10] attributed the elasticity to the entanglement of PEO chains, which is expected to increase with temperature. Two factors can be identified as pivotal in the thermally driven transition: the formation of ordered domains and the entanglements or interpenetration of PEO chains, as illustrated in Fig. 1. The viscoelasticity of the system and the corresponding microstructural description are strictly correlated. Costanzo et al. [11] discussed the origin of elasticity of these compact, micellar structures, suggesting that their results may explain interpenetration and, as such, elasticity.

The interpenetration of PEO chains could result from the growth of larger micelles or an increase in their number. Although direct experimental evidence is lacking, the contribution of enhanced interpenetration of PEO chains in the outer coronas of adjacent micelles appears reasonable, as already discussed by Costanzo et al. [11]. SAXS data indicate that while the PPO core swells with temperature, the overall micellar radius remains unchanged. However, this observation provides limited insight into interpenetration mechanisms and is influenced by the fit model adopted to calculate these quantities and various error sources. As explained in Sect. 4.1, the estimation of the overall micellar radius in the BCC phase is in fact the result of geometric considerations, assuming that the micelles are in contact on the cubic unit diagonal.

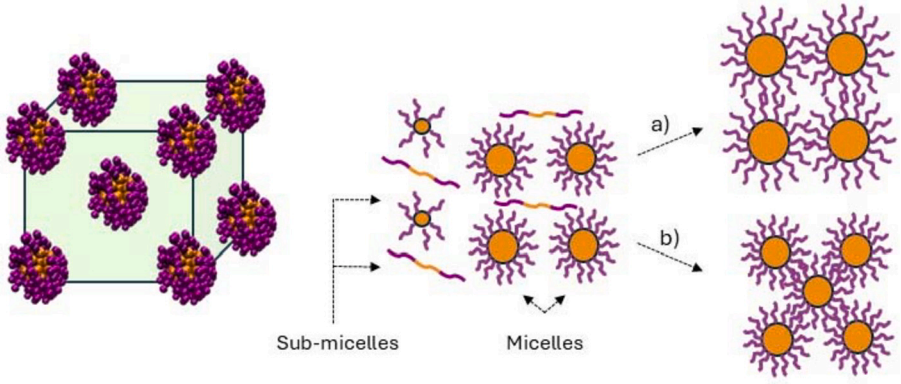

Fig. 1. Schematic diagram of two mechanisms: a) interpenetration of PEO chains resulting from the growth of larger micelles; b) interpenetration due to an increase in the number of micelles (Figure reproduced from Ref. [10]).

The outline of the article is as follows. Section 2 briefly describes the experimental techniques employed. Section 3 introduces the DPD approach along with the model adopted to represent the system in DPD. Section 3.3 explains how the morphological and rheological characterization is performed in DPD. Section 3.4 describes the computational details and illustrates the setup of the simulations carried out. The results are presented and discussed with the conclusions provided in Section 4.

2. Materials and techniques for experimental investigation

2.1. Materials

45 wt% Pluronic F68 (Sigma-Aldrich, St. Louis, MO) water solution was prepared at room temperature by means of magnetic stirring. Pluronic F68 was dispersed in cold double-distilled water [12], and kept at 5 °C for a few days.

2.2. Experimental methodologies

The experimental data used to validate the simulations were obtained by adopting rheology and Small-Angle X-ray Scattering (SAXS). Rheological experiments were performed using a rotational stress-controlled rheometer DHR-2 (Discovery Hybrid Rheometer, TA Instruments, USA) with 40 mm sandblasted parallel plates. A Peltier unit was used for temperature control. The linear viscoelasticity of the systems was studied through frequency sweep tests at lower and higher temperatures. Preliminary strain sweep tests were conducted at different temperatures to detect the linear viscoelastic regime. A strain of 0.1% was used for all dynamic tests. Low viscosity silicon oil was employed as a solvent trap to avoid water evaporation.
Experimental details of the SAXS measurements are already presented elsewhere [13,6]. All experiments were repeated at least three times.

3. Models and methods for computational modeling

3.1. Dissipative particle dynamics: a coarse-grained technique

Dissipative Particle Dynamics (DPD), introduced by Hoogerbrugge and Koelman in 1992 [14], provides a robust simulation technique that operates at larger time and length scales than traditional molecular dynamics. This makes it particularly well suited for studying the self-assembly and rheological behavior of tri-block copolymers, such as F68, in water mixtures. In fact, this simulation approach captures both the relevant molecular details of the nanoscopic building blocks and their supramolecular organization while simultaneously resolving the system's hydrodynamic behavior over extended time scales. In DPD, groups of atoms or molecules are treated as single entities, known as *beads*. The *beads* interact via a mesoscopic force field. The DPD force field consists of variables in reduced units, the so-called DPD units. Typically in DPD, the mass of a single DPD *bead*, the conservative cutoff radius, and the thermal energy are taken as, respectively, mass, time, and energy units. The motion of each *bead* is governed by Newton's second law:

$$\frac{d\boldsymbol{r}_i}{dt} = \boldsymbol{v}_i, \quad \frac{d\boldsymbol{v}_i}{dt} = \frac{\boldsymbol{f}_i}{m_i}, \tag{1}$$

with $i = 1, .., N$; $\boldsymbol{r}_i$ and $\boldsymbol{v}_i$ are the position and velocity of the *bead* i with mass m_i, respectively, and N is the number of DPD *beads* in the system. The force $\boldsymbol{f}_i$ acting on the i-th *bead* is the sum of three pairwise contributions:

$$\boldsymbol{f}_i = \sum_{j \neq i} (\boldsymbol{F}_{ij}^C + \boldsymbol{F}_{ij}^D + \boldsymbol{F}_{ij}^R), \tag{2}$$

where the sum runs over the *beads* indices contained in the closest vicinity to the *bead* i within a certain cutoff radius. The conservative contribution, $\boldsymbol{F}_{ij}^C$, is a soft-repulsive force acting between a pair of *beads* i and j and having the following functional form:

$$\boldsymbol{F}_{ij}^C = \begin{cases} a_{ij}\left(1 - \dfrac{r_{ij}}{r_c^C}\right)\hat{\boldsymbol{r}}_{ij}, & r_{ij} < r_c^C \\ 0, & r_{ij} \geq r_c^C \end{cases} \tag{3}$$

where a_{ij} denotes a maximum repulsion between *beads* i and j, $r_{ij} = |\boldsymbol{r}_{ij}| = |\boldsymbol{r}_i - \boldsymbol{r}_j|$ is the separation distance between a pair of *beads*, $\hat{\boldsymbol{r}}_{ij} = \boldsymbol{r}_{ij}/r_{ij}$ is the unit vector of the *bead-bead* separation distance and r_c^C is the cutoff radius for the conservative interactions. Pluronic chains are represented employing the *bead-and-spring* model where neighboring *beads* interact through a harmonic potential given by:

$$E_{harm} = K_b(r_{ij} - r_0)^2, \tag{4}$$

where r_0 is the nominal equilibrium distance and K_b the harmonic constant. In the DPD model, the degrees of freedom eliminated during the Coarse-Graining (CGing) are effectively reintroduced through the inclusion of pairwise dissipative and random forces. The dissipative and random forces, $\boldsymbol{F}_{ij}^D$ and $\boldsymbol{F}_{ij}^R$, respectively, represent the effect of viscous drag and the thermal and vibrational energy of the system. The expressions for general dissipative and random forces can then be written as

$$\boldsymbol{F}_{ij}^D = -\gamma w^D(r_{ij})(\hat{\boldsymbol{r}}_{ij} \cdot \boldsymbol{v}_{ij})\hat{\boldsymbol{r}}_{ij}, \tag{5}$$

$$\boldsymbol{F}_{ij}^R = \sigma w^R(r_{ij}) \frac{\xi_{ij}}{\sqrt{\Delta t}} \hat{\boldsymbol{r}}_{ij}. \tag{6}$$

Here, γ is the dissipative parameter and σ is the noise parameter; $\boldsymbol{v}_{ij} = \boldsymbol{v}_i - \boldsymbol{v}_j$, ξ_{ij} represents a random variable with zero mean value and unit variance and Δt is the simulation time step. The dissipative and noise parameters are related to each other in order to satisfy the fluctuation-dissipation theorem (FDT):

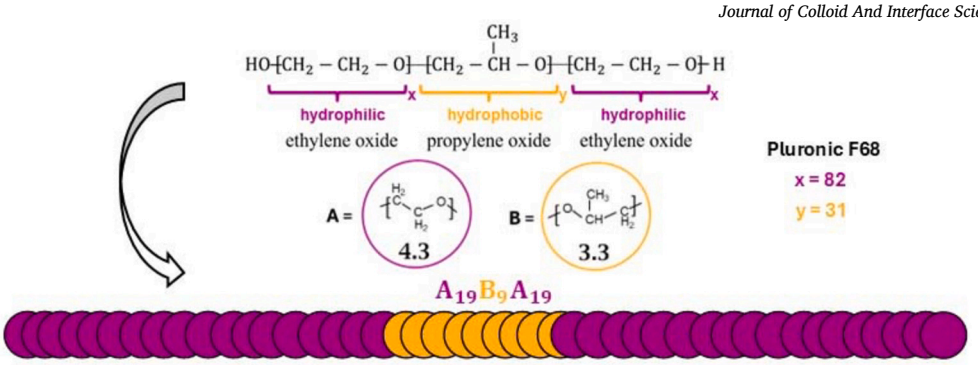

Fig. 2. Molecular structure and coarse-grained model of the F68 macromolecule.

$$\sigma = \sqrt{2k_B\theta\gamma}, \tag{7}$$

where k_B denotes the Boltzmann constant and θ the system temperature. The weight functions $w^D(r_{ij})$ and $w^R(r_{ij})$ define the dependence of the dissipative and random forces, respectively, on the *bead-bead* separation distance. These functions are related by the following equation:

$$w^D(r_{ij}) = [w^R(r_{ij})]^2. \tag{8}$$

The dissipative and random forces act together as a thermostat and, along with the conservative one, also guarantee local momentum conservation and ensure correct hydrodynamic behavior. This work incorporates recent advances into the DPD model. Although the original DPD model has long been valued for enabling microscale systems to equilibrate within a reasonable simulation time, the corresponding dynamic path does not always reflect the actual one.

A key limitation arises in the description of transport properties: the standard DPD framework does not accurately capture those of real fluids. To address this point, the dissipative weight function $w^D(r_{ij})$ is treated as a Generalized Weighting Function (GWF), following the approach proposed by Fan et al. [15], which has been previously used in our studies. It is defined as:

$$w^D(r_{ij}) = \left[w^R(r_{ij})\right]^2 = \begin{cases} \left(1 - \dfrac{r_{ij}}{r_c^D}\right)^{2s} \hat{\mathbf{r}}_{ij}, & r_{ij} < r_c^D \\ 0 & r_{ij} \geq r_c^D \end{cases} \tag{9}$$

where r_{ij} is the *bead-bead* separation distance and r_c^D is the cutoff distance and its exponent, $s \in (0, 1]$, plays an important role in modeling of dynamic properties of a DPD fluid along with γ and r_c^D. This modification treats the exponent of the weighting function, s, as a free parameter and the dissipative cutoff radius, r_c^D, as independent of the conservative one, r_c^C. In the standard formulation $s = 1$ and $r_c^C = r_c^D$. This extension introduces in the model adjustable parameters to calibrate transport properties. Adjusting γ, s and r_c^D to experimental values of self-diffusivity and viscosity [16,17], DPD can capture realistic solvent dynamics at the mesoscale level without undesired effects on the nature of the phase assumed by the simulated system. In fact, the equilibrium behavior of the system is governed exclusively by conservative forces since the time averages of the dissipative and fluctuation forces are zero. However, an accurate description of the dissipative forces is essential to capture realistic dynamics. Another important limitation of the original version of the DPD model is the artificial crossing of polymer chains, which leads to inaccurate rheological behavior, such as stress-strain curves and responses to external stimuli. To address this, the mSRP (modified Segmental Repulsive Potential) is incorporated into the DPD model to improve its ability to reproduce both non-equilibrium and equilibrium behavior [18]. The introduction of the mSRP prevents non-physical bond crossings caused by the soft repulsive interactions inherent in the standard DPD model. The rheological properties are governed by the physical crossing of chains. To avoid non-physical increases in viscosity, it is essential to isolate and account only for the physical contributions within the simulation [19–23]. The mSRP introduces a repulsive interaction force between non-adjacent bonds, which takes a form similar to the conservative force through which these bonds interact:

$$\mathbf{F}_{kl}^{SRP} = b\left(1 - \frac{d_{kl}}{d_c}\right)\hat{\mathbf{d}}_{kl}\,, \tag{10}$$

where $\mathbf{F}_{kl}^{SRP}$ is the force acting between the bonds k and l separated by distance d_{kl}; b e d_c are respectively the force constant and the bond-bond cutoff distance. The distance between the two bonds is calculated as the distance between the midpoints of the bonds. This formulation of the SRP has recently been shown to be the most effective in maintaining chain topology [18].

3.2. Model and parameters

Pluronic F68 macromolecules are represented by 47 *beads* chains, where CG EO *bead* contains 4.3 atomistic EO monomers, and the CG PO *bead* contains 3.3 atomistic EO monomers. These CG factors have been used already in other works [24] following the *mapping* scheme described by van Vlimmeren et al. [25]. As a result, all beads are intended to represent almost the same mass and volume [26,14,27,28]. The DPD topology of the chain can be schematically represented as $A_{19}B_9A_{19}$, where A and B correspond to the EO and PO *beads*, respectively as shown in Fig. 2. The repulsion parameter between similar *beads* is determined to ensure that the compressibility in the simulation model matches the compressibility of the liquid to be studied [17] according to the following relationship:

$$a_{ii} = \frac{\kappa^{-1} - k_B\theta}{2\alpha\rho}, \tag{11}$$

where α is a constant, κ^{-1} is the dimensionless bulk modulus at the considered temperature (the inverse of dimensionless compressibility), ρ is the number density and θ is the system temperature. In particular, this formulation adopts the generalized method proposed in [29], which we thoroughly assessed in our earlier study [17]. This method incorporates both the simulation temperature θ and the temperature-dependent compressibility κ to determine the repulsive interaction parameter. Therefore, the parameters a_{WW}, a_{AA} and a_{BB} vary with temperature according to Eq. (11). The repulsion parameters between *beads* of different types, a_{ij}, can be estimated using the relation [28]:

$$a_{ij} \approx a_{ii} + 3.27\chi_{ij}. \tag{12}$$

As shown in Eq. (12), the strength of interaction between dissimilar *beads* includes an additional term reflecting the increased repulsion due to the solubility dissimilarity. The χ_{ij} parameters are taken from the literature [30]. However, the resulting conservative parameters are then fine-tuned to reproduce the experimental radii of both the core and the corona of the micelle at T = 25 °C. The repulsive parameters a_{AW}

and a_{BW} are treated as temperature-dependent parameters. They describe the hydrophobicity of PEO and PPO blocks, respectively. The hydrophobicity of these blocks is a function of temperature and plays a crucial role in the micellization of the F68 polymer in water. In particular, the difference in hydrophobicity between PEO and PPO blocks at different temperatures is a key factor in determining the micellization process, influencing both the characteristics and arrangement of the resulting micelles. The higher the hydrophobicity, the higher the parameters a_{AW} and a_{BW}. Specifically, as the temperature increases, a_{AW} and a_{BW} increase with temperature to reflect changes in the way the hydrophobic block interacts with other species. According to Alexandris et al. [31], the hydrophobic block of Pluronic induces micellization due to the weakening of the hydrogen bonding between water and the PPO block as temperature increases. As a result, the interaction parameters for PEO-water and PPO-water increase with temperature to account for the increased hydrophobicity, as already discussed in other work [32]. For *beads* that are directly connected in the chain, the parameters r_0 (the nominal equilibrium distance) and K_b (the harmonic constant) are set to ensure that the bond lengths follow the desired distribution.
The details on the calibration of the DPD model parameters at different temperatures are provided in Sect. 1 of Supporting Information.

3.3. Morphological and rheological properties from DPD

3.3.1. Cluster analysis to determine morphological properties

A post-processing routine analyzes the self-assembly and morphology of the DPD simulation trajectories at different temperatures.
Pluronic aggregates (micelles) are identified: two macromolecules are grouped into the same aggregate if they share a minimum number of contact pairs. A contact pair refers to two *beads* belonging to separate macromolecules that are within a specific distance of each other [33]. After this step the aggregation number, A_s, and its mass distribution are computed. The aggregation or association number, indicated by A_s, refers to the number of individual chains forming a single aggregate, which will also be denoted by i in the following. To characterize the distribution of aggregates of varying sizes, the weight distribution function of aggregation numbers, F_w, is introduced. It is defined as:

$$F_w(i) = \frac{m_i N_i}{\sum_{i=1}^{\infty} m_i N_i}, \tag{13}$$

where $m_i = m_{A_s,i}$ represents the weight of an aggregate with an association number $A_s = i$ and $N_i = N_{A_s,i}$ denotes the number of aggregates with that association number. This function quantifies the weighted fraction of aggregates with a specific aggregation number present in the system. To enable comparison with experimental data, the weight-averaged aggregation number is calculated using the expression:

$$\langle A_s \rangle_w = \frac{\sum_i m_i^2}{\sum_i m_i}, \tag{14}$$

where m_i is the weight of an aggregate i. The micelle radius, denoted as R_g^M, is computed as the radius of gyration of the aggregate. The latter is defined as the square root of the mean square distance of the beads in a chain or aggregate from its center of mass, r_{CM}, assuming uniform mass distribution among the particles:

$$\langle R_g^2 \rangle = \frac{1}{N} \sum_{i=1}^{N} (\boldsymbol{r}_i - \boldsymbol{r}_{CM})^2, \tag{15}$$

where N is the number of particles that form the chain or aggregate. Eventually, the micelle and PPO core radii are computed using the gyration tensor, $\boldsymbol{S}$. It serves as a practical descriptor of the shape and size of the aggregates, which describes the second moments of the position vectors of the *beads*:

$$S_{mn} = \frac{1}{N} \sum_{i=1}^{N} (r_i^m - r_{\mathrm{CM}}^m)(r_i^n - r_{\mathrm{CM}}^n), \tag{16}$$

where r_i^m stands for the m-th Cartesian coordinate of $\boldsymbol{r}_i$ and r_{CM} is the m-th Cartesian coordinate of $\boldsymbol{r}_{\mathrm{CM}}$. The gyration tensor is a symmetric matrix which can be diagonalized:

$$\boldsymbol{S} = \begin{pmatrix} \lambda_x^2 & 0 & 0 \\ 0 & \lambda_y^2 & 0 \\ 0 & 0 & \lambda_z^2 \end{pmatrix}, \tag{17}$$

where λ_x^2, λ_y^2 and λ_z^2 are eigenvalues chosen so that $\lambda_x^2 < \lambda_y^2 < \lambda_z^2$. The eigenvectors define the main directions of the aggregate, while the eigenvalues correspond to the gyration lengths, representing the extent of the aggregate along each of these directions. The eigenvalues are used to calculate various shape descriptors of the aggregates, such as the radius of gyration:

$$R_g^2 = \lambda_x^2 + \lambda_y^2 + \lambda_z^2. \tag{18}$$

Similarly to the aggregation number, the weight-averaged radius of gyration is calculated to enable comparison with experimental data. The same calculation applies to the entire micelle to obtain the radius of the micelle $\langle R_g^{\mathrm{OUT}} \rangle$, and to the PPO core alone to obtain $\langle R_g^{\mathrm{PPO}} \rangle$.

3.3.2. Non-equilibrium simulations to determine rheological properties

The viscoelastic properties are investigated by applying a non-equilibrium oscillatory shear technique [34]. This approach, often referred to as the "box deforming technique", mimics a real experimental procedure by imposing the corresponding flow condition on the simulation box. It is fundamentally analogous to the Lees-Edwards boundary conditions, the most widely used method to impose shear flow [35–38]. This technique utilizes the SLLOD equations of motion, imposing a velocity profile that varies with time throughout the domain [39]. This profile results from the application of a sinusoidal strain:

$$\epsilon(t) = \epsilon_0 \sin(\omega t), \tag{19}$$

where ϵ_0 is the amplitude of the oscillation and ω is the angular frequency. At the beginning of the simulation, all beads are assigned an initial average velocity profile that matches the instantaneous deformation rate of the simulation box. This approach accelerates the establishment of the desired flow regime. Typically, in a viscoelastic material, the stress response $\sigma(t)$ exhibits oscillations at the same frequency as the applied strain:

$$\sigma(t) = \sigma_0 \sin(\omega t + \delta). \tag{20}$$

However, a phase angle shift δ occurs, ranging from 0 in the case of ideal elastic behavior to $\pi/2$ for purely viscous behavior. The stress can be further decomposed into two orthogonal functions:

$$\sigma(t) = \epsilon_0 [G'(\omega) \sin(\omega t) + G''(\omega) \cos(\omega t) \tag{21}$$

such that one of them is in sync with the imposed strain and the other has a $\pi/2$ phase lead. Comparing Eq. (20) and Eq. (21), the elastic and storage moduli can be defined as follows:

$$G' = \frac{\sigma_0}{\epsilon_0} \cos\delta \tag{22}$$

$$G'' = \frac{\sigma_0}{\epsilon_0} \sin\delta. \tag{23}$$

A major challenge of this approach is the strong noise in the $\sigma(t)$ time series, leading to intense fluctuations [40]. To address this, a data processing strategy is employed that combines pre-averaging of the $\sigma(t)$ signal and discrete Fourier transform analysis, as applied in previous studies [40].

3.4. Computational details and simulation setup

DPD equilibrium and non-equilibrium simulations were performed using the open-source software LAMMPS [41]. Specifically, this work

employed the in-house implemented `dpd/ext pair_style` in LAMMPS to apply the modified model defined in Sect. 3.1. The necessary source code can be accessed via our github account (https://github.com/mulmopro/LAMMPS-DPD-EXT), while the post-processing of the DPD trajectories was performed using a dedicated tool.

DPD equilibrium simulations were performed to investigate the self-assembly behavior of F68/water mixtures at 45 wt% at different temperatures. In this work, five temperatures were considered: 5 °C, 25 °C, 28 °C, 40 °C, and 70 °C.

A system of $N = 192.000$ identical particles with $m_i = m = 1$ was simulated in a cubic box of length equal to $40r_c^C$ with periodic boundary conditions in all directions. The number density was set to $\rho = 3$.

Here, a temperature scaling method is employed, previously applied to liquid water in our earlier work [17] and other studies [23,42]. The reference temperature $T_R = 298.15$ K was used to scale all the investigated temperatures T. Consequently, the simulation temperature $\theta = T/T_R$ ranged from 0.933 to 1.22. Once the temperature scale was defined, the DPD fluid interaction parameters were consistently adjusted with the simulation temperature θ. The conservative repulsive parameter, a_{WW}, was defined as a temperature-dependent parameter as explained in Sect. 3.2. a_{AA} and a_{BB} were assumed to be equal to a_{WW}. The interaction parameters between various types of polymer *beads* were modeled also as temperature-dependent, as described in Sect. 3.2. Equilibrium trajectories obtained at different temperatures are analyzed using a post-processing tool to compute both system-wide properties such as pair correlation functions and per-aggregate properties such as shape descriptors. Quantitative characterization of supramolecular aggregates is crucial for understanding the microstructure mechanisms that govern rheological properties at different temperatures.

The rheological properties were then computed under non-equilibrium conditions using the oscillatory shear technique at the investigated temperatures. The tilt factor oscillated sinusoidally with the specified amplitude and period.

4. Results and discussion

The following sections present experimental and computational results, comparing simulations with experiments to reveal how the morphological behavior influences the macroscopic rheology of the Pluronic F68 aqueous system at different temperatures.

4.1. Experiments

The 45 wt% Pluronic F68 aqueous solution was investigated through experimental methodologies, namely, rheology and Small-Angle X-ray Scattering (SAXS), to detect its viscoelastic properties and extract microstructural information. Fig. 3a reports the linear frequency sweeps of the investigated sample at various temperatures (5-70 °C). The complex modulus, G*, is reported as a function of frequency. Fig. 11, black points in Sect. 4.2, shows the values of G* in Fig. 3a at 100 rad/s, in a way to highlight the transition temperature from a liquid-like behavior to a solid one. Indeed, whilst at low temperatures the frequency response is typical of a liquid-like system, as the temperature increases the overall viscosity rises, until it abruptly increases and reaches a solid-like phase. The liquid to solid transition starts at roughly 35 °C, as previously discussed [43,11]. The dynamic frequency sweep tests at 70 °C provide a description of the systems in their crystallized form. Fig. 3b shows the linear frequency response at 70 °C of the 45 wt% Pluronic F68 sample. The viscoelastic moduli, G' (storage modulus) and G'' (loss modulus), are reported as a function of frequency. The frequency response in Fig. 3b is representative of a viscoelastic network, with a well-defined crossover angular frequency (i.e. highlighted by the red dashed line) and a pronounced elasticity.

SAXS measurements at different temperatures allow for accessing the assembly of the system at the nanometer length scale by following its

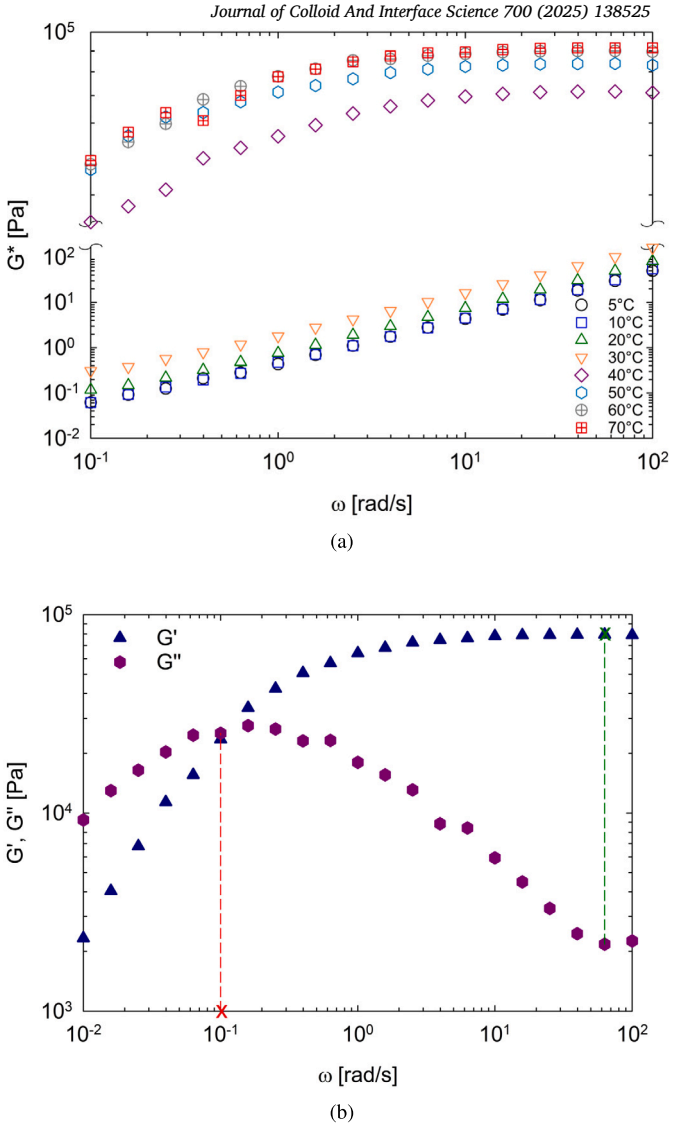

Fig. 3. Linear frequency responses of the 45 wt% Pluronic F68 aqueous solution. Measurements at various temperatures (a). Response at 70 °C, with the crossover angular frequency and plateau modulus indicated by the red and green dashed lines (b).

microstructural thermally-driven evolution. Furthermore, microstructural quantitative information on the Pluronic self-assemblies can be extracted. As an example, Fig. 4 shows the SAXS profiles of the investigated system at 5, 20, 25, 30, and 70 °C. The figure contains new and already published data from [13,6]. At 5 °C, a featureless SAXS profile indicates the absence of any self-assemblies. At such a temperature, Pluronic F68 is dispersed in water as single unimers. At 20 and 25 °C, a broad correlation peak reveals the presence of disordered micellar structures. At 30 and 70 °C, SAXS profiles show a BCC phase, depicted by Bragg peaks at q^*, $\sqrt{2}q^*$, and $\sqrt{3}q^*$ ($q^* \approx 0.64\,\mathrm{nm}^{-1}$). The self-assembly of Pluronic F68 from unimers to spherical micelles and, then, to a BCC phase with increasing temperature is consistent with literature data.

The solid lines in Fig. 4 represent the SAXS data fits performed by means of models available in the SasView package.

The micellar phase was modeled as monodisperse and homogeneous spheres (form factor), interacting through a hard sphere potential (structure factor) [44,13]. The corresponding fitting parameters, i.e., the apparent micellar core radius, R_{PPO}, and the hard-sphere radius, R_{OUT}, are reported in Table 1.

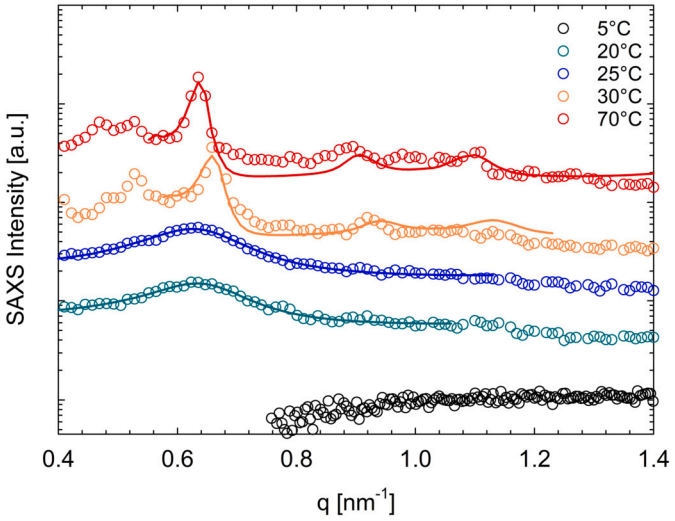

Fig. 4. SAXS intensity profiles of the 45 wt% Pluronic F68 water solution, at different temperatures. Solid lines represent the fit to the data by means of models in the SasView Package. Curves are vertically shifted for better visualization. The figure contains new and already published data [6,13].

Table 1
Model parameters extracted from the fit to SAXS profiles. Error estimates are reported in the table.

Temperature [°C]	Morphology	R_{PPO} [nm]	R_{OUT} [nm]	a [nm]
5	Unimeric phase	—	—	—
20	Micellar phase	4.2 ± 0.1	5.0 ± 0.1	—
25	Micellar phase	4.0 ± 0.1	5.0 ± 0.1	—
30	BCC phase	5.8 ± 0.2	5.8 ± 0.1	13.4 ± 0.1
70	BCC phase	6.1 ± 0.1	6.0 ± 0.1	13.9 ± 0.1

The BCC phase was modeled with a paracrystalline model of hard spheres in a BCC lattice of infinite size (lattice parameter a) [45,13]. The corresponding fitting parameters, i.e., a and R_{PPO} are listed in Table 1 along with R_{OUT}, that is here estimated as $R_{OUT} = \sqrt{3}a/4$, assuming the micellar aggregates in contact on the cubic unit diagonal.

The fit to SAXS profiles provides information on the characteristic dimension of the Pluronic nanoassemblies, i.e., spherical micelles and BCC lattice. On the one hand, SAXS analysis provides robust description about the thermally-driven morphological evolution of the system; on the other hand, such an investigation relies on models and various error sources, including assumptions on the BCC nanostructural parameters, micelles with perfectly spherical shape, micelles in contact on the cubic unit diagonal, etc. Moreover, X-rays do not probe the effective radius of the PPO core but a larger core radius, which also contains a scarcely swollen PEO layer [13]. As such, computational tools come to the aid of such a study, strongly supporting the experimental analysis and providing fundamental information.

4.2. Simulation results

The 45 wt% Pluronic F68 water solution was simulated through DPD equilibrium and non-equilibrium simulations across different temperatures to detect respectively microstructure and resulting rheological properties. The experimental rheological data presented in the previous section reveal a liquid-to-solid transition around 35 °C, where the system adopts the characteristics of a soft solid. It behaves as a non-Newtonian material, exhibiting well-defined viscoelasticity and relaxation time.
Microstructural analysis of DPD trajectories complements the experimental observations by providing a deeper understanding of the structural organization and mechanisms that govern the elasticity. By monitoring key parameters, such as the number of aggregates and their

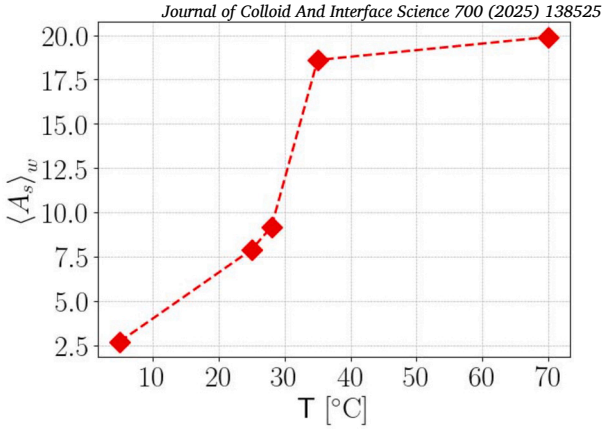

Fig. 5. Weight-average aggregation number $\langle A_s \rangle$ as a function of temperature. Error estimates are reported in Supplementary Material.

average aggregation number per single micelle at different temperatures, simulations offer valuable insight into the evolution of micellar interactions.
The microstructure analysis tool tracks the evolution of the number and size of the aggregates in the simulation box, revealing how the self-assembly process varies with temperature. Aggregates are classified as micellar or sub-micellar based on a cut-off aggregation number, enabling a detailed assessment of how their population shifts with temperature.
Fig. 5 illustrates the average aggregation number over the examined temperature range. In the Supporting Information the total number of aggregates (sub-micelles and micelles) over the examined temperature range is also detailed. They show that from 5 to 25 °C, sub-micelles decrease in number as they contribute to the formation of micelles. Instead, between 25 and 28 °C, sub-micelles continue to decrease as they support the growth of existing micelles, as indicated by an increase in the average aggregation number and a nearly constant micelle count. Further temperature increase induces a sharp decrease in sub-micelles, which eventually disappear. The total number of aggregates is then essentially made up of micelles.
The weight-averaged distribution functions at different temperatures offer deeper insight into the aggregation behavior and support a more comprehensive interpretation of the previous plots. The distribution at 5 °C (Fig. 6a) shows no peak, indicating the absence of aggregates large enough to be classified as micelles. Increasing the temperature to 25 °C (Fig. 6b), leads to the appearance of a peak, which indicates the presence of micelles.
The distribution function and average properties reveal that the system, at this stage, consists of both sub-micelles and micelles of varying sizes undergoing continuous fluctuations. This promotes the formation of a disordered domain, leading to a viscous macroscopic behavior. The disordered nature of the system is evident in the snapshot shown in Fig. 7a, while the associated rheological behavior is examined in the next paragraph. When the temperature reaches 28 °C (Fig. 6c), the distribution function shows little change, reflecting the continued growth of the micelles. By 40 °C (Fig. 6d), the distribution becomes sharply compact, indicating that the micelles are uniform in size and tightly packed. They remain stationary around their positions, promoting the formation of an ordered domain. The close proximity of the micelles favors the interpenetration of PEO chains. The ordered domain is clearly evident in the snapshot shown in Fig. 7b. The corresponding rheological properties will be discussed in the next paragraph. In addition, the micelle and PPO core radii are computed at different temperatures and compared with experimental results, specifically with Small-Angle X-ray Scattering (SAXS) data. The experimental results in Fig. 8c reveal that the radius of the micelle remains nearly constant, while the radius of the core shows a slight increase as the temperature rises. As a result, the PEO shell radius slightly decreases with increasing temperature. These

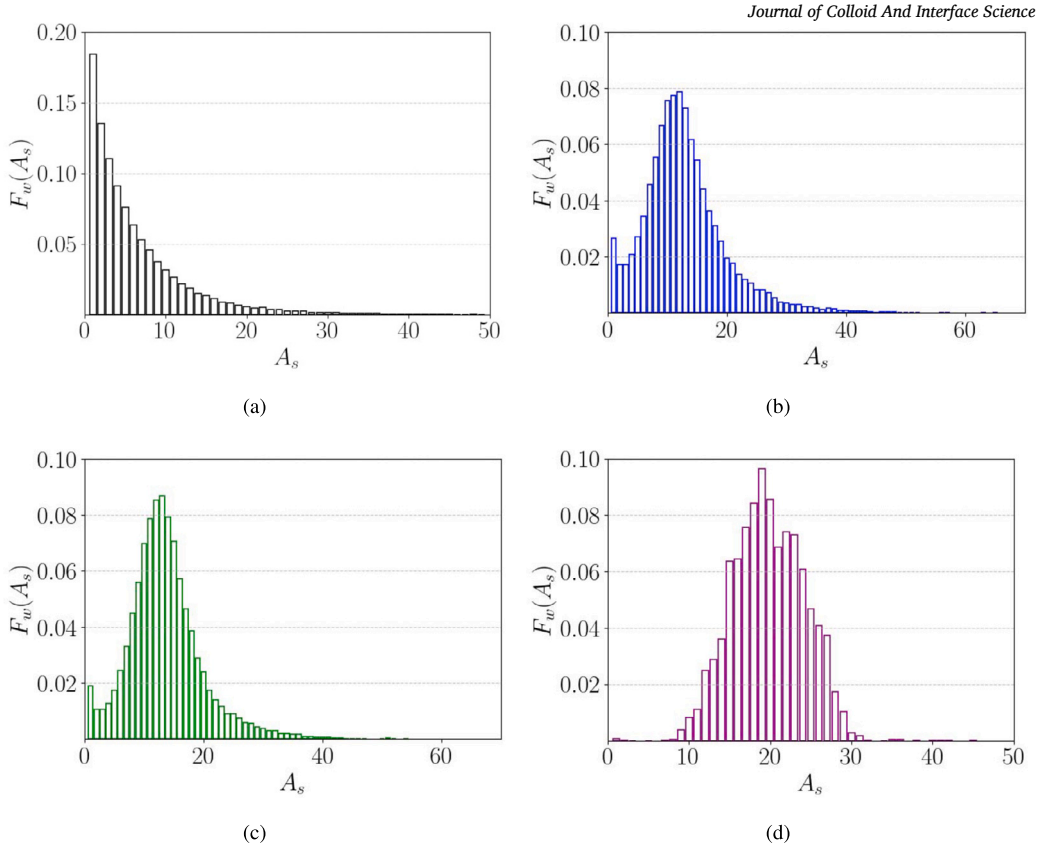

Fig. 6. Weight-averaged distribution functions at different temperatures: (a) $T = 5\,°C$; (b) $T = 25\,°C$; (c) $T = 28\,°C$ and (d) $T = 40\,°C$.

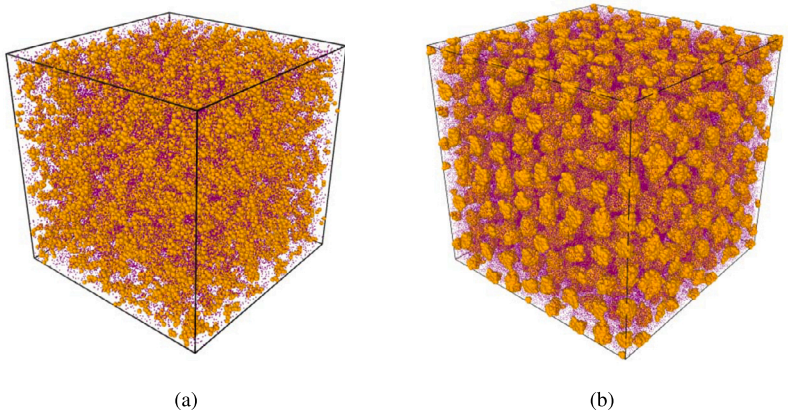

Fig. 7. Snapshots of microstructure of F68 wt% at different temperatures: (a) $T = 5\,°C$ and (b) $T = 40\,°C$.

values are compared with the values calculated in Fig. 8b. Given the uncertainty associated with both the experimental and the simulated parameters, the agreement is quite good at lower temperatures. However, as the temperature increases, a discrepancy arises. Simulations predict an increase in the radius of the micelle, while the PPO core remains nearly constant. This suggests an expansion of the PEO shell. This simulation evidence is crucial for understanding the rheological behavior of the experimentally observed system. As discussed previously, the interaction between chains may provide the microstructural basis for the observed viscoelasticity and relaxation time. Eventually, the RDFs at different temperatures (Fig. 9) are computed for different species, to obtain insights into their spatial configuration. These calculations confirm the change in microstructural order with temperature. The PPO-PPO RDF is the most significant, displaying the appearance of a periodicity in the peaks increasing the temperature, which demonstrates the transition from a disordered to an ordered domain.

The viscoelastic properties of 45 wt% Pluronic F68 water solution at different temperatures were also measured by imposing an oscillatory shear. The value $\epsilon_0 = 0.1$ was selected based on previous studies [46,47], which demonstrated that this strain amplitude lies well within the linear viscoelastic regime, where the complex moduli remain independent of the strain magnitude. The resulting stress response is also sinusoidal, with the same frequency as the applied strain but exhibiting a phase shift that characterizes the viscoelastic behavior of the material. Given that the applied strain amplitude remains within the linear viscoelastic regime, we consider its effect on the mesoscale structure to be negligible. This assumption is justified by the qualitative nature of the analysis, which aims to capture the temperature-induced emergence of elasticity. Data processing for the stress output from SAOS is performed to smooth out the noise and assess that the stress response oscillates with the same

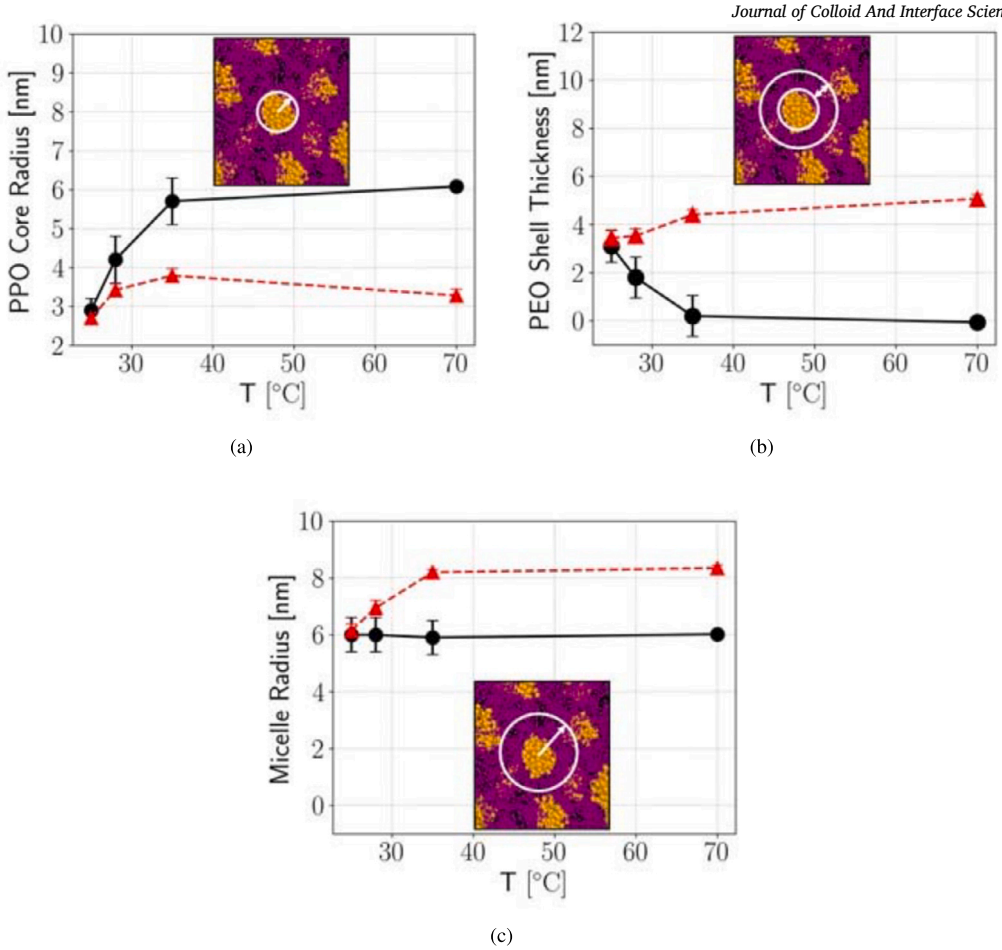

Fig. 8. Predicted structural features of micelles as functions of temperature: (a) PPO core radius, (b) PEO shell thickness, and (c) micelle radius. Red points represent simulation results, and black points represent experimental data [11,6].

frequency as the strain input. A moving average technique is applied to pre-average the stress signal. The window size is carefully chosen based on a sensitivity analysis, where it is progressively increased to prevent the data from being overly smeared. A discrete Fourier transform is then applied to the pre-averaged stress output [40].

Figs. 10 and 11 show, respectively, the dependence of the loss, storage, and complex moduli as a function of temperature. The results are reported in DPD units. The trends for the storage modulus (G') and the loss modulus (G'') align with experimental evidence. Specifically, the elastic component remains close to zero at 5 °C, 25 °C, and 28 °C, then shows a step-like increase around 40 °C, consistent with the observed behavior. The loss modulus increases with increasing temperature, as expected. In fact, a closer packing of micelles will also greatly enhance inter-micellar friction, resulting in a high value of G''. The complex modulus undergoes an order-of-magnitude increase near 40 °C.

5. Conclusions

In this work, we demonstrated that Dissipative Particle Dynamics (DPD) is a powerful computational approach for investigating the interplay between morphology and rheology in Pluronic systems, providing deeper insight into the mechanisms underlying their thermoresponsive behavior. Our simulations effectively captured the temperature-induced liquid-to-solid transition in a 45 wt% Pluronic F68/water mixture. The formation of a body-centered cubic (BCC) phase was consistently observed at elevated temperatures in both the DPD simulations and experimental results, which confirms the reliability of the model.

By integrating simulation and experimental approaches, we achieved a coherent and complementary understanding of the structural evolution of the system, i.e. core and shell sizes of the micellar self-assembly and its viscoelastic response. These findings are particularly relevant for drug delivery applications, where control over the morphology and mechanical properties is crucial for carrier performance.

In contrast to earlier studies that typically addressed morphology and rheology separately, our approach bridges these aspects to provide a comprehensive picture of the thermoresponsive behavior of Pluronic systems. In addition, few studies have explored the temperature effects on the rheology of such systems using DPD; here, we employ it not only to capture thermally induced morphological transitions but also to directly explain the experimentally observed rheological response. This unified framework is particularly valuable for temperature-sensitive drug delivery applications, where both structure and mechanics must be finely controlled.

The methodology proposed lays the foundation for future simulation campaigns involving pharmaceutical molecules, ultimately supporting the design of smart nanocarriers with tunable release profiles. In fact, the framework developed in this study provides a foundation for ongoing investigations into drug-loaded Pluronic systems. Although the integration of pharmaceutical molecules is the subject of a separate, more detailed study, the insights presented here are essential to interpret how these additives influence the morphology and mechanical properties of micellar. This work provides the essential basis for the integration of drug molecules into the DPD scheme and will guide the rational design of nanocarriers for temperature-sensitive drug delivery applications. In our recent works [3,5,13], we observed that Pluronic F68 acts as a very efficient depot for huge amounts of an anti-inflammatory drug. As such, further study is under way and future simulation campaigns incorporating specific drug molecules within the DPD scheme will support the

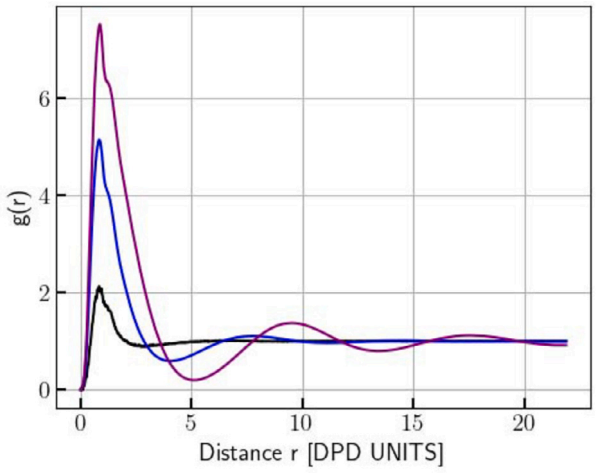

(a)

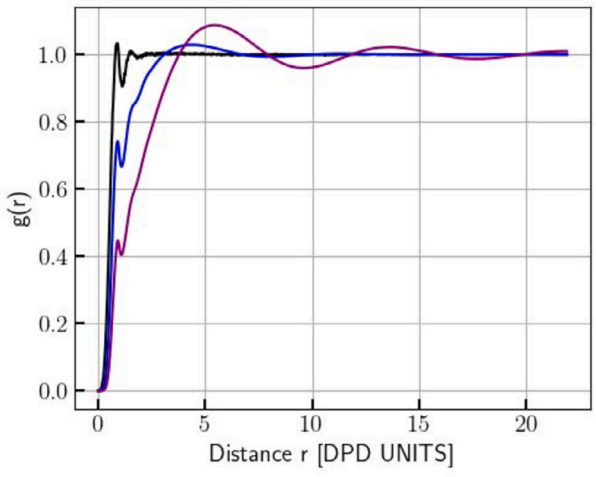

(b)

Fig. 9. Radial distribution functions (RDFs) for PPO-PPO interactions (a) and PPO-Water interactions (b) at three temperatures: black ($T = 5\,°C$), blue ($T = 25\,°C$), and purple ($T = 40\,°C$).

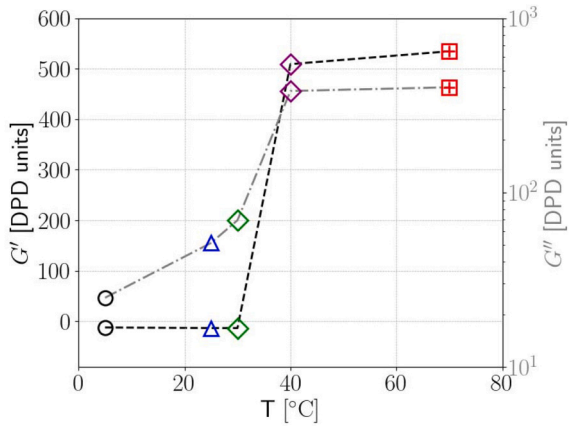

Fig. 10. Computed values of the elastic modulus G' (points on dashed black line) and the loss modulus G'' (points on the dashed gray line) as function of temperature. Symbols at different temperatures are represented with different colors.

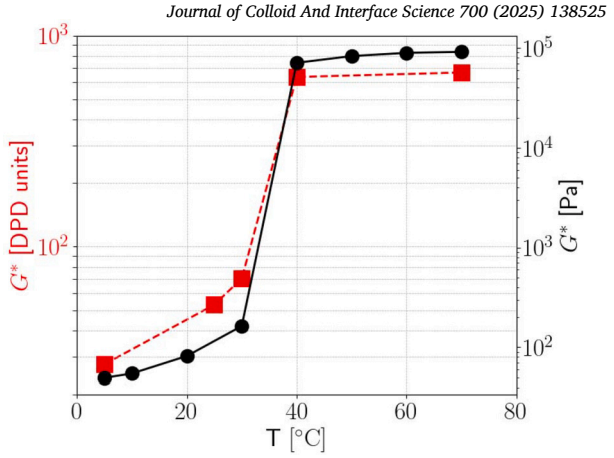

Fig. 11. Computed (red square points) and experimental (black circle points) values of the complex modulus G^* in DPD units across different temperatures.

rational design of advanced nanocarriers with customized release profiles, thus advancing the field of controlled drug delivery.

CRediT authorship contribution statement

N. Lauriello: Writing – review & editing, Writing – original draft, Software, Methodology, Investigation, Formal analysis, Data curation, Conceptualization. **N.A. Di Spirito:** Writing – review & editing, Writing – original draft, Methodology, Investigation, Formal analysis, Data curation, Conceptualization. **Karel Šindelka:** Writing – review & editing, Software, Methodology, Conceptualization. **G. Boccardo:** Writing – review & editing, Supervision, Conceptualization. **R. Pasquino:** Writing – review & editing, Supervision, Methodology, Investigation, Formal analysis, Conceptualization. **N. Grizzuti:** Writing – review & editing, Supervision, Methodology, Formal analysis, Conceptualization. **D. Marchisio:** Writing – review & editing, Supervision, Project administration, Methodology, Funding acquisition, Formal analysis, Conceptualization.

Declaration of competing interest

The authors declare that they have no known competing financial interests or personal relationships that could have appeared to influence the work reported in this paper.

Acknowledgements

Computational resources were provided by HPC@POLITO. We acknowledge the CINECA award under the ISCRA initiative, for the availability of high-performance computing resources and support. The financial support from ICSC (Centro Nazionale di Ricerca in High Performance Computing, Big Data and Quantum Computing, funded by European Union - NextGenerationEU) is also gratefully acknowledged. This study was carried out within the «Non-equilibrium self-assembly of structured fluids: a multi-scale engineering problem» project – funded by European Union – Next Generation EU within the PRIN 2022 program (Project No. 2022JJRH8H) (D.D. 104 - 02/02/2022 Ministero dell'Università e della Ricerca).

Appendix A. Supplementary material

Supplementary material related to this article can be found online at https://doi.org/10.1016/j.jcis.2025.138525.

Data availability

Data will be made available on request.

References

[1] N.A. Di Spirito, N. Grizzuti, R. Pasquino, Self-assembly of Pluronics: a critical review and relevant applications, Phys. Fluids 36 (11) (2024) 111302.
[2] M. Karimi, H. Droghetti, D. Marchisio, Multiscale modeling of expanding polyurethane foams via computational fluid dynamics and population balance equation, Macromol. Symp. 1 (2016) 108–122.
[3] N.A. Di Spirito, C. Di Baia, N. Grizzuti, R. Pasquino, B. De Gennaro, Drug release from Pluronic F68 hydrogels, Phys. Fluids 3 (2024) 1544–1554.
[4] L. Yang, P. Alexandridis, Physicochemical aspects of drug delivery and release from polymer-based colloids, Curr. Opin. Colloid Interface Sci. 5 (1) (2000) 132–143.
[5] N.A. Di Spirito, N. Grizzuti, M. Casalegno, F. Castiglione, R. Pasquino, Phase transitions of aqueous solutions of Pluronic F68 in the presence of diclofenac sodium, Int. J. Pharm. (2023) 123353.
[6] N.A.D. Spirito, F. Auriemma, O.R.D. Ballesteros, N. Grizzuti, R. Pasquino, A pluronic block copolymer in h2o and d2o: the isotope effect on phase transition, Phys. Fluids 36 (2024) 121712.
[7] B. Nyström, H. Walderhaug, Dynamic viscoelasticity of an aqueous system of a poly(ethylene oxide)–(propylene oxide)–(ethylene oxide) triblock copolymer during gelation, J. Phys. Chem. 100 (13) (1996) 5433–5439.
[8] B. Nyström, A.-L. Kjøniksen, Dynamic light scattering of a poly(ethylene oxide)–(propylene oxide)–(ethylene oxide) triblock copolymer in water, Langmuir 13 (17) (1997) 4520–4526.
[9] S. Hvidt, E.B. Joergensen, W. Brown, K. Schillen, Micellization and gelation of aqueous solutions of a triblock copolymer studied by rheological techniques and scanning calorimetry, J. Phys. Chem. 98 (47) (1994) 12320–12328.
[10] B.K. Lau, Q. Wang, W. Sun, L. Li, Micellization to gelation of a triblock copolymer in water: thermoreversibility and scaling, J. Polym. Sci., Part B, Polym. Phys. 42 (10) (2004) 2014–2025.
[11] S. Costanzo, A. Di Sarno, M. D'Apuzzo, P.R. Avallone, E. Raccone, A. Bellissimo, F. Auriemma, N. Grizzuti, R. Pasquino, Rheology and morphology of pluronic f68 in water, Phys. Fluids 33 (4) (2021) 043113.
[12] I.R. Schmolka, Artificial skin i. Preparation and properties of pluronic f-127 gels for treatment of burns, J. Biomed. Mater. Res. 6 (6) (1972) 571–582.
[13] N.A. Di Spirito, N. Grizzuti, V. Lutz-Bueno, G. Urciuoli, F. Auriemma, R. Pasquino, Pluronic F68 micelles as carriers for an anti-inflammatory drug: a rheological and scattering investigation, Langmuir 2 (2024) 1544–1554.
[14] P.J. Hoogerbrugge, J.M.V.A. Koelman, Simulating microscopic hydrodynamic phenomena with dissipative particle dynamics, Europhys. Lett. 19 (1992) 155–160.
[15] X. Fan, N. Phan-Thien, S. Chen, X. Wu, T.Y. Ng, Simulating flow of dna suspension using dissipative particle dynamics, Phys. Fluids 18 (6) (2006) 063102.
[16] N. Lauriello, J. Kondracki, A. Buffo, G. Boccardo, M. Bouaifi, M. Lísal, D. Marchisio, Simulation of high Schmidt number fluids with dissipative particle dynamics: parameter identification and robust viscosity evaluation, Phys. Fluids (2021) 073106.
[17] N. Lauriello, M. Lísal, G. Boccardo, D. Marchisio, A. Buffo, Modeling temperature-dependent transport properties in dissipative particle dynamics: a top-down coarse-graining toward realistic dynamics at the mesoscale, J. Chem. Phys. 161 (2024) 034112.
[18] T.W. Sirk, Y.R. Slizoberg, J.K. Brennan, M. Lisal, J.W. Andzelm, An enhanced entangled polymer model for dissipative particle dynamics, J. Chem. Phys. 136 (13) (2012) 134903.
[19] Y. Araki, N. Arai, Dissociation effect of non-covalent bond for morphological behavior of triblock copolymers: a dissipative particle dynamics study, Chem. Eng. Commun. 208 (1) (2019) 1–13.
[20] T.W. Sirk, Y.R. Sliozberg, J.K. Brennan, M. Lisal, J.W. Andzelm, An enhanced entangled polymer model for dissipative particle dynamics, J. Chem. Phys. 136 (13) (2012) 134903.
[21] G. Dorenbos, Coarse-grained study of the effect of hydrophobic side chain length on cluster size distributions and water diffusion in (amphiphilic-hydrophobic) multiblock co-polymer membranes, Polymer 173 (2019) 43–57.
[22] R. Ketkaew, Y. Tantirungrotechai, Dissipative particle dynamics study of swcnt reinforced natural rubber composite system: an important role of self-avoiding model on mechanical properties, Macromol. Theory Simul. 27 (9) (2018) 1700093.
[23] Z. Li, Y.-H. Tang, H. Lei, B. Caswell, G.E. Karniadakis, Energy-conserving dissipative particle dynamics with temperature-dependent properties, J. Comput. Phys. (2014) 113–127.
[24] N. Lauriello, D.N. Ponnana, Z. Ma, K. Šindelka, A. Buffo, G. Boccardo, D. Marchisio, W. Pan, Interpretable machine-learning enhanced parametrization methodology for pluronics–water mixtures in dpd simulations, Soft Matter (2025).
[25] B.A.C. van Vlimmeren, N.M. Maurits, A.V. Zvelindovsky, G.J.A. Sevink, J.G.E.M. Fraaije, Simulation of 3D Mesoscale Structure Formation in Concentrated Aqueous Solution of the Triblock Polymer Surfactants (Ethylene Oxide)13(Propylene Oxide)30(Ethylene Oxide)13 and (Propylene Oxide)19(Ethylene Oxide)33(Propylene Oxide)19. Application of Dynamic Mean-Field Density Functional Theory, ACS Publications, 1999.
[26] P. Durchschlag, H. Zipper, Calculation of the partial volume of organic compounds and polymers, Prog. Colloid & Polym. Sci. 94 (1994) 20–39.
[27] P. Español, P. Warren, Statistical mechanics of dissipative particle dynamics, Europhys. Lett. 30 (4) (1995) 191–196.
[28] R.D. Groot, P.B. Warren, Dissipative particle dynamics: bridging the gap between atomistic and mesoscopic simulation, J. Chem. Phys. 11 (1997) 4423–4435.
[29] P. Vanya, J. Sharman, J.A. Elliott, Invariance of experimental observables with respect to coarse-graining in standard and many-body dissipative particle dynamics, J. Chem. Phys. 150 (6) (2019) 064101.
[30] S.L. Guo, T.J. Hou, X.J. Xu, Simulation of the phase behavior of the (EO)13(PO)30(EO)13(Pluronic L64)/water/p-xylene system using MesoDyn, J. Phys. Chem. B 106 (43) (2002) 11397–11403.
[31] P. Alexandridis, T.A. Hatton, Poly(ethylene oxide)-poly(propylene oxide)-poly(ethylene oxide) block copolymer surfactants in aqueous solutions and at interfaces: thermodynamics, structure, dynamics, and modeling, Colloids Surf. A 96 (1995) 1–46.
[32] A. De Nicola, T. Kawakatsu, G. Milano, A hybrid particle-field coarse-grained molecular model for pluronics water mixtures, Macromol. Chem. Phys. 214 (17) (2013) 1940–1950.
[33] K. Šindelka, M. Lísal, Interplay between surfactant self-assembly and adsorption at hydrophobic surfaces: insights from dissipative particle dynamics, Mol. Phys. 119 (15–16) (2021) e1857863.
[34] W. Hong, J. Lin, X. Tian, L. Wang, Distinct viscoelasticity of hierarchical nanostructures self-assembled from multiblock copolymers, Macromolecules 53 (24) (2020) 10955–10963.
[35] Y.R. Sliozberg, J.W. Andzelm, J.K. Brennan, M.R. Vanlandingham, V. Pryamitsyn, V. Ganesan, Modeling viscoelastic properties of triblock copolymers: a DPD simulation study, J. Polym. Sci., Part B, Polym. Phys. 1 (2010) 15–25.
[36] P. Xu, J. Lin, L. Zhang, Distinct viscoelasticity of nanoparticle-tethering polymers revealed by nonequilibrium molecular dynamics simulations, J. Phys. Chem. C 121 (50) (2017) 28194–28203.
[37] Y. Chen, Z. Li, S. Wen, Q. Yang, L. Zhang, C. Zhong, L. Liu, Molecular simulation study of role of polymer–particle interactions in the strain-dependent viscoelasticity of elastomers (payne effect), J. Chem. Phys. 141 (10) (2014) 104901.
[38] M.P. Allen, D.J. Tildesley, Computer Simulation of Liquids, Clarendon Press, Cambridge, UK, 1987.
[39] D.J. Evans, G.P. Morriss, Nonlinear-response theory for steady planar Couette flow, Phys. Rev. A 30 (3) (1984) 1528–1530.
[40] O. Adeyemi, S. Zhu, L. Xi, Equilibrium and non-equilibrium molecular dynamics approaches for the linear viscoelasticity of polymer melts, Phys. Fluids 34 (5) (2022) 053107.
[41] A.P. Thompson, H.M. Aktulga, R. Berger, D.S. Bolintineanu, W.M. Brown, P.S. Crozier, P.J. in 't Veld, A. Kohlmeyer, S.G. Moore, T.D. Nguyen, R. Shan, M.J. Stevens, J. Tranchida, C. Trott, S.J. Plimpton, Lammps - a flexible simulation tool for particle-based materials modeling at the atomic, meso, and continuum scales, Comput. Phys. Commun. (2022) 108171.
[42] E. Mayoral, A.G. Goicochea, Modeling the temperature dependent interfacial tension between organic solvents and water using dissipative particle dynamics, J. Chem. Phys. 138 (9) (2013) 094703.
[43] Y.L. Wu, R. Sprik, W.C.K. Poon, E. Eiser, Effect of salt on the phase behaviour of f68 triblock peo/ppo/peo copolymer, J. Phys. Condens. Matter 18 (2006) 4461–4470.
[44] M. Kotlarchyk, S.H. Chen, Analysis of small angle neutron scattering spectra from polydisperse interacting colloids, J. Chem. Phys. 79 (1983) 2461–2469.
[45] E. Eiser, F. Molino, G. Porte, O. Diat, Nonhomogeneous textures and banded flow in a soft cubic phase under shear, Phys. Rev. E 61 (2000) 6759–6764.
[46] J.G.H. Cifre, S. Hess, M. Kröger, Linear viscoelastic behavior of unentangled polymer melts via non-equilibrium molecular dynamics, Macromol. Theory Simul. 13 (9) (2004) 748–753.
[47] M. Vladkov, J.-L. Barrat, Linear and nonlinear viscoelasticity of a model unentangled polymer melt: molecular dynamics and rouse modes analysis, Macromol. Theory Simul. 15 (3) (2006) 252–262.